Analytical Methods

RSC Publishing

PAPER

View Article Online
View Journal | View Issue

Hierarchical Cu–Co–Ni nanostructures electrodeposited on carbon nanofiber modified glassy carbon electrode: application to glucose detection†

Cite this: *Anal. Methods*, 2013, **5**, 6360

Hongyu Liu,[a] Xingping Lu,[a] Dejian Xiao,[a] Minxian Zhou,[a] Dujian Xu,[a] Lanlan Sun[b] and Yonghai Song*[a]

Hierarchical Cu–Co–Ni nanostructures (Cu–Co–Ni NSs) attached to carbon nanofibers (CNFs) modified glassy carbon electrode (GCE) was prepared by electrodeposition. Scanning electron microscopy results indicated that many hierarchical Cu–Co–Ni NSs were formed and uniformly dispersed on the CNFs/GCE surface. The electrochemical behavior and electrocatalytic performance of the Cu–Co–Ni NSs/CNFs/GCE towards the oxidation of glucose were evaluated by cyclic voltammograms, chronoamperometry and amperometric methods. The results revealed that Cu–Co–Ni NSs/CNFs/GCE has a good electrocatalytic activity for glucose oxidation and could be used as a nonenzymatic glucose sensor. The sensor showed an acceptable linear range from 0.01 to 4.30 mM with a sensitivity of 104.68 μA mM cm^{-2}, and a detection limit of 3.05 μM ($S/N = 3$). The good catalytic activity, high sensitivity, good selectivity and stability rendered the Cu–Co–Ni NSs/CNFs/GCE to be a promising electrode for constructing a nonenzymatic glucose sensor.

Received 15th July 2013
Accepted 22nd August 2013

DOI: 10.1039/c3ay41170b

www.rsc.org/methods

1. Introduction

Glucose determination is a focused research area that receives extensive attention because of its importance in the fields of biotechnology, clinical diagnostics, and food industry applications,[1] especially in the treatment and management of diabetes. Diabetes is one of the common diseases causing death and disability. It has been found that diabetic patients have high concentrations of glucose in their blood. The number of patients has increased in recent years, thus, a fast, easy and low-cost method to monitor the concentration of blood glucose daily is urgently needed. Among the various analytical techniques for quantitative detection of glucose,[2–5] electrochemistry techniques have been extensively applied because of advantages such as low cost, high stability, simple preparation, easy miniaturization and automation.[6] Due to their high selectivity, electrochemical biosensors based on the electrocatalysis of immobilized glucose oxidase to glucose oxidation have been widely developed.[7–10] However, crucial disadvantages in developing enzymatic glucose sensors are: (1) the loss of enzyme activity that occurs during the immobilization and (2) the activity of enzyme is easily affected by temperature, oxygen, pH, humidity, detergents, organic reagents and toxic chemicals.[11,12] Therefore, the development of nonenzymatic glucose sensors has become more and more important, because of their potential for higher sensitivity and stability as well as their reduced susceptibility to fouling by enzyme-aging and adsorbed intermediates.[13]

Over the past decades, developments in the field of nanotechnology and material science have paved the way for the synthesis of numerous new materials with desired morphologies and physicochemical properties.[14] Recently, metal or metal oxide micro/nanomaterials have received extensive attention for their promising sensing applications.[15–22] In particular, due to the enhanced catalytic performances over traditional monometallic micro/nanomaterials, bimetallic or trimetallic micro/nanomaterials such as Au–Pd,[23] Ag–Ni,[24,25] Cu–Co,[26,27] Pt–Pd–Co,[28,29] Pt–Ni–Co,[30] *etc.* exhibited synergetic behaviors such as specific electrocatalytic activity, more active sites and improved long-term stability. Most of the noble metallic and poly-noble metallic composites exhibited the superior electro-oxidation behavior of glucose.[23–30] However, in order to lower the cost of glucose detection, some cheaper transition metal and poly-transition metal composites are worthy of further study.

It has been reported that the combination of metal micro/nanomaterials with carbon materials such as graphene, carbon nanotubes, carbon nanofibers (CNFs), *etc.* is capable of

[a]*Key Laboratory of Functional Small Organic Molecules, Ministry of Education, College of Chemistry and Chemical Engineering, Jiangxi Normal University, Nanchang 330022, People's Republic of China. E-mail: yhsonggroup@hotmail.com; Fax: +86 791 88120862; Tel: +86 791 88120862*

[b]*State Key Laboratory of Luminescence and Applications, Changchun Institute of Optics, Fine Mechanics and Physics, Chinese Academy of Sciences, 3888 East Nan-Hu Road, Changchun 130033, People's Republic of China*

† Electronic supplementary information (ESI) available. See DOI: 10.1039/c3ay41170b

enhancing the optical, electrical and magnetic properties of the metal micro/nanomaterials, thereby resulting in improved selectivity, stability and sensing performances.[31,32] For example, Guo *et al.* developed a facile solution-phase self-assembly method to deposit FePt nanoparticles (NPs) on graphene as an enhanced catalyst for oxygen reduction.[31] Huang *et al.* demonstrated the fabrication of low-defect multi-walled carbon nanotubes supported PtCo NPs for electro-oxidation of methanol.[32] To the best of our knowledge, there are few research reports on the trimetal micro/nanostructures deposited on CNFs surface for nonenzymatic glucose detection.

In this work, low-cost Cu, Co, Ni metal salts were chosen as the polymetallic source to construct hierarchical Cu–Co–Ni nanostructures (NSs) by simply electrodepositing them onto a CNFs modified glassy carbon electrode (GCE). The morphology of the Cu–Co–Ni NSs was controllable by tuning the deposition time and the ratio of Cu, Co and Ni. The as-prepared hierarchical Cu–Co–Ni NSs/CNFs/GCE exhibited good electrocatalytic activity to glucose oxidation and was developed into a nonenzymatic glucose sensor. The effects of the preparation conditions of Cu–Co–Ni NSs/CNFs/GCE on glucose detection were investigated in detail.

2. Experimental

2.1. Reagents and chemicals

Polyacrylonitrile (PAN, M_w 269 000 g mol^{-1}) and *N*,*N*-dimethylformamide (DMF) were purchased from Sigma-Aldrich (St Louis, USA). Nickel chloride ($NiCl_2 \cdot 6H_2O$) and copper chloride ($CuCl_2$) were obtained from China National Pharmaceutical Group Chemical Reagent Factory. Chloride hexahydrate ($CoCl_2 \cdot 6H_2O$), sodium sulfate anhydrous (Na_2SO_4), cetyl trimethyl ammonium bromide ($CH_3(CH_2)_{15}N(CH_3)_3Br$, CTAB) and sodium hydroxide (NaOH) were purchased from Tianjin FuChen Chemical Reagent Factory (Tianjin, China). Other reagents were purchased from Beijing Chemical Reagent Factory (Beijing, China). All chemicals were of analytical grade and used as received without further purification. 0.1 M NaOH was directly used as the electrolyte solution (pH 13). The other solutions were prepared with ultra-pure water purified by a Millipore-Q System ($\rho \geq 18.2$ MΩ cm).

2.2. Preparation of modified electrode

CNFs were prepared according to a previous method.[33] The CNFs have a diameter ranging from 300 to 600 nm and a length of tens of micrometers. The GCE was polished carefully with 1.0, 0.3 and 0.05 μm alumina slurry on felt pads and then cleaned by brief ultrasonication. 2 mg of CNFs were added into 20 mL of ultra-pure water and sonicated for 30 min. 10 μL of the suspension was dropped onto the cleaned GCE surface and subsequently dried at room temperature. A precursor solution (10 mL) of 10 mM $CoCl_2 \cdot 6H_2O$, 10 mM $NiCl_2 \cdot 6H_2O$, 10 mM $CuCl_2$ and 100 mM Na_2SO_4 were used as the polymetal NSs source. A constant potential of −1.1 V (*vs.* saturated calomel electrode (SCE)) was applied to the CNFs/GCE (no stirring). The optimal deposition time was determined to be 900 s. All experimental solutions were deoxygenated by high-purity nitrogen for at least 15 min.

2.3. Apparatus

The scanning electron microscopy (SEM) analysis was carried out using a XL30 ESEM-FEG SEM at an accelerating voltage of 20 kV equipped with a Phoenix energy dispersive X-ray analyzer (EDXA). All electrochemical measurements were performed on a CHI 750D electrochemical workstation (Shanghai, China) at ambient temperature. A three-electrode configuration was used with the modified or bare GCE electrodes as the working electrode, a SCE as the reference electrode, and a platinum wire as the auxiliary electrode. The cyclic voltammetric experiments were performed in a quiescent solution. The amperometric experiments were carried out under continuous stirring. 0.1 M NaOH as the supporting electrolyte solution was purged with high purity nitrogen for 15 min prior to each measurement and then a nitrogen atmosphere was kept over the solution during measurements.

3. Results and discussion

3.1. Electrodeposition of Cu–Co–Ni NSs on CNFs/GCE

Cyclic voltammograms (CVs) were utilized to monitor the electrodeposition process of Cu–Co–Ni NSs. Fig. 1 showed the CVs of the CNFs/GCE in a potential range from 0.8 V to −1.2 V, in which a cathodic peak at −1.05 V (peak III) indicated that Co^{2+} and Ni^{2+} were reduced on the CNFs/GCE surface to form Co–Ni NSs.[34,35] The anodic peak at −0.20 V (peak IV) was attributed to the dissolution of the deposited metal NSs.[36] The cathodic peaks at −0.03 V (peak I) and −0.37 V (peak II) were related to the reduction of Cu^{2+} into Cu^{+} and Cu NSs formation, respectively. The anodic peak at 0.52 V (peak V) was attributed to the dissolution of the deposited Cu NSs.[37] With the increasing of scan cycles, the cathodic peak current gradually decreased, and the peak potential shifted positively (as indicated by the black vertical arrow in Fig. 1), indicating that Co^{2+}, Ni^{2+} and Cu^{2+} were gradually reduced into the metal atom on the CNFs/GCE surface. In addition, the thickness of Cu–Co–Ni NSs films could be controlled by tuning the deposition time,[34] which was discussed in the following section in detail.

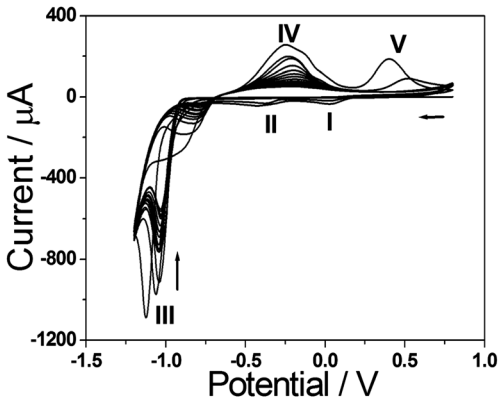

Fig. 1 CVs of CNFs/GCE in 20 mM $CoCl_2 \cdot 6H_2O$, 10 mM $NiCl_2 \cdot 6H_2O$, 2.5 mM $CuCl_2$ and 0.1 M Na_2SO_4 at 0.1 V s^{-1}.

3.2. Characteristics of the as-prepared Cu–Co–Ni NSs/CNFs/GCE

The SEM technique was used to characterize the morphologies of the Cu NSs, Co NSs, Ni NSs and Cu–Co–Ni NSs. Fig. 2A showed the SEM image of the Cu NSs/CNFs/GCE, which indicated that flower-like Cu structures were formed over the surface of CNFs. Fig. 2B showed the SEM image of the Co NSs/CNFs/GCE, in which the flower-like Co nanosheets formed a rough surface on the CNFs surface. Fig. 2C showed the SEM image of the Ni NSs/CNFs/GCE, in which many granular Ni NSs were formed and covered the CNFs surface completely. Fig. 2D showed the SEM image of the Cu–Co–Ni NSs/CNFs/GCE (the concentration ratio of Cu^{2+} : Co^{2+} : Ni^{2+} was 2.5 mM : 20 mM : 10 mM, the deposition potential was −1.1 V (*vs.* SCE) and the deposition time was 900 s), in which the granular and hierarchical Cu–Co–Ni NSs were dispersed on the CNFs surface to form a three-dimensional (3D) structure. In contrast, the SEM image of Cu–Co–Ni NSs/GCE was investigated in Fig. S1.† The Cu–Co–Ni NSs/GCE has little 3D hierarchical Cu–Co–Ni alloy NSs unlike that of Cu–Co–Ni NSs/CNFs/GCE, which might result in the poor electrochemical properties, and the amount of nanostructure of Cu–Co–Ni NSs/GCE is less than that of Cu–Co–Ni NSs/CNFs/GCE. To investigate the growth mechanism of the 3D hierarchical Cu–Co–Ni polymetallic NSs, EDXA was used to determine the components of the Cu–Co–Ni NSs/CNFs/GCE (Fig. 2E). It revealed Cu, Co, Ni, C and O as the constituting elements (C comes from the CNFs/GCE). The ratio of the Cu : Co : Ni was evaluated to be about 1 : 6 : 3, which is similar to the molar ratio of the Cu^{2+} : Co^{2+} : Ni^{2+} in solution (inset of Fig. 2E). Meanwhile, Fig. 2F showed the SEM elemental mapping image, in which the elements of Cu, Co, Ni are marked with blue, red and green, respectively. The uniform distribution of three colors indicated the uniform distribution of Cu, Co, Ni elements in the 3D hierarchical Cu–Co–Ni polymetal NSs. The results revealed that the obtained composite was Cu–Co–Ni alloy NSs rather than the Cu, Co, Ni respective structures with phase separation.

The morphologies of Cu–Co–Ni NSs/CNFs/GCE with different deposition time were also investigated by SEM. Fig. 3A–F showed the SEM images of the NSs with the corresponding deposition time of 0 s, 10 s, 40 s, 600 s, 900 s and 1200 s. Without the electrodeposition of metal NSs, the long-strip CNFs film was formed, which contained many interspaces to reveal a large surface (Fig. 3A). With the increase of

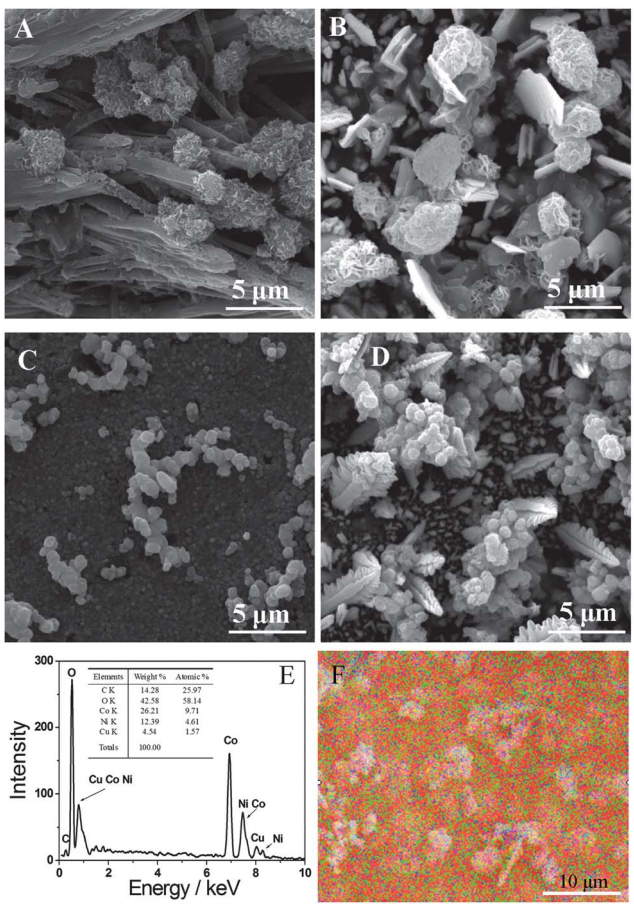

Fig. 2 SEM images of Cu NSs/CNFs/GCE (A), Co NSs/CNFs/GCE (B), Ni NSs/CNFs/GCE (C) and Cu–Co–Ni NSs/CNFs/GCE (D). EDXA of Cu–Co–Ni NSs/CNFs/GCE (E), inset is the constituting element table. (F) SEM elemental mappings of Cu–Co–Ni NSs/CNFs/GCE.

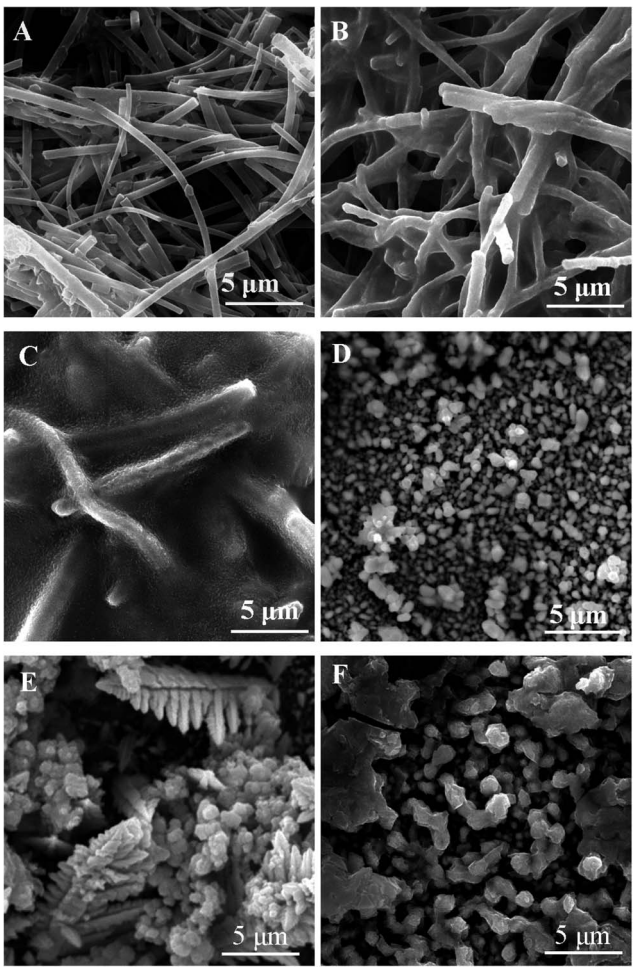

Fig. 3 SEM of Cu–Co–Ni NSs/CNFs/GCE with different deposition times: (A) 0 s, (B) 10 s, (C) 40 s, (D) 600 s, (E) 900 s and (F) 1200 s.

deposition time, more metal NSs were formed over the CNFs surface and the interspaces decreased gradually (Fig. 3B). After 40 s, the CNFs were covered with a uniform metal film and only a few CNFs could be observed as shown in Fig. 3C. When the deposition time was increased to 600 s, the metal gradually grew to form some tiny granular Cu–Co–Ni NSs and the CNFs were completely covered (Fig. 3D). Up to 900 s, the metal NSs grew to form some uniform particles and the hierarchical Cu–Co–Ni alloy NSs, which provided a rough 3D structure and a large specific surface area (Fig. 3E). When the time was further increased to 1200 s (Fig. 3F), only Cu–Co–Ni alloy NPs combined with a little thick film were observed, while the hierarchical Cu–Co–Ni alloy NSs disappeared. Therefore, the morphologies and thickness of alloy metal Cu–Co–Ni NSs could be controlled by tuning the deposition time, and this indicated that the hierarchical Cu–Co–Ni NSs exhibited the largest surface area when the deposition time was 900 s.

3.3. Electrochemical behavior of Cu–Co–Ni NSs/CNFs/GCE

Since the concentration of metal ion might determine the amount of metal in the Cu–Co–Ni NSs/CNFs/GCE system, the effect of the concentration of Cu^{2+}, Co^{2+}, Ni^{2+} as the polymetallic source to construct hierarchical Cu–Co–Ni NSs on the CVs response of Cu–Co–Ni NSs/CNFs/GCE was also investigated, and the results were shown in Fig. 4. Fig. 4A showed the effect of Cu^{2+} concentration on the anodic peak current and cathodic peak current of Cu–Co–Ni NSs/CNFs/GCE. The peak current increased with the increase of Cu^{2+} concentration from 1 mM to 2.5 mM and then decreased with further increase of Cu^{2+} concentration. The maximum peak current response occurred at 2.5 mM Cu^{2+}. Besides, the effects of Co^{2+} and Ni^{2+} concentration on the CVs of the Cu–Co–Ni NSs/CNFs/GCE were also investigated, as shown in Fig. 4B and C. The maximum peak current response occurred at 20 mM Co^{2+} and 10 mM Ni^{2+}, respectively. Therefore, at 2.5 mM Cu^{2+}, 20 mM Co^{2+} and 10 mM Ni^{2+}, the peak current showed the maximum response.

The deposition time of the Cu–Co–Ni NSs also played an important role in the electrochemical behavior of Cu–Co–Ni NSs/CNFs/GCE. The effect of the deposition time on the peak current of the Cu–Co–Ni NSs/CNFs/GCE in 0.1 M N_2-saturated NaOH solution at 0.1 V s^{-1} was shown in Fig. 4D. The peak currents increased as the deposition time was increased from 300 s to 1200 s owing to the continuous increase of the amount of Cu–Co–Ni alloy NSs under the continuous deposition. However, the CVs response obtained under 1500 s was lower than that of 1200 s, which is in accordance with the morphologies change in Fig. 3. The excessive Cu–Co–Ni NSs formed some thick Cu–Co–Ni film and NPs on the surface of electrode. The peak currents of the Cu–Co–Ni NSs/CNFs/GCE obtained under deposition time of 900 s was similar to that of 1200 s, but the peak potential separation (ΔE_p) under 1200 s was wider than that of 900 s, which indicated a slower electron transfer for Cu–Co–Ni NSs/CNFs/GCE. Therefore, the deposition time of 900 s was chosen as the optimal experimental condition.

The effect of the potential scan rates on the electrochemical performance of the Cu–Co–Ni NSs/CNFs/GCE was shown in Fig. 5A. It is obvious that the redox peak current increased linearly with increasing of the potential scan rate from 100 to 300 mV s^{-1} (Fig. 5B), indicating a quasi-reversible surface-controlled electrochemical process. The electron-transfer

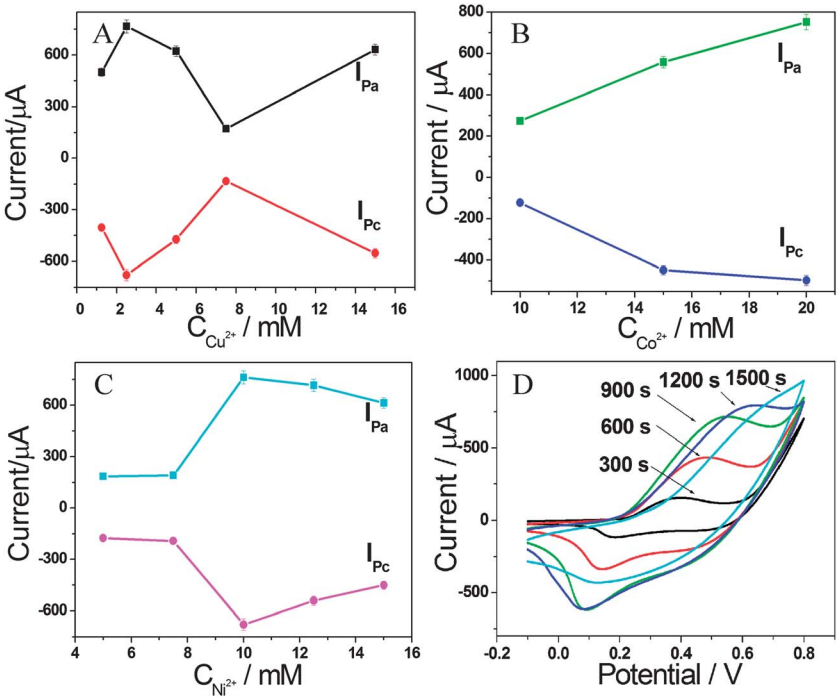

Fig. 4 Effects of the concentration of Cu^{2+} (A), Co^{2+} (B) and Ni^{2+} (C) on the peak current of the Cu–Co–Ni NSs/CNFs/GCE in 0.1 M N_2-saturated NaOH solution at 0.1 V s^{-1}. (D) Effects of the deposition time on the peak current of the Cu–Co–Ni NSs/CNFs/GCE in 0.1 M N_2-saturated NaOH solution at 0.1 V s^{-1}.

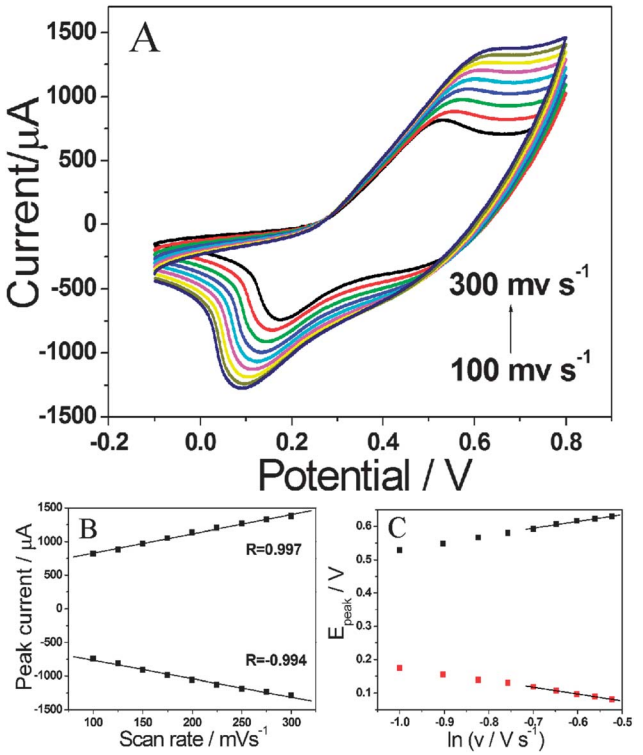

Fig. 5 (A) CVs of the Cu–Co–Ni NSs/CNFs/GCE 0.1 M N_2-saturated NaOH solution at various scan rates from 100 to 300 mV s^{-1}. (B) Plot of peak current *versus* scan rates. (C) Plot of peak potential *versus* the logarithm of scan rates.

coefficient (α_s) and electron-transfer rate constant (k_s) could be determined based on Laviron theory:[38]

$$E_{pc} = E^{o'} + \frac{RT}{\alpha_s nF} - \frac{RT}{\alpha_s nF}\ln v \quad (1)$$

$$E_{pa} = E^{o'} + \frac{RT}{(1-\alpha_s)nF} + \frac{RT}{(1-\alpha_s)nF}\ln v \quad (2)$$

where n is the electron transfer number, R is the gas constant ($R = 8.314$ J mol^{-1} K^{-1}), T is the temperature in Kelvin ($T = 298$ K) and F is the Faraday constant ($F = 96\,493$ C mol^{-1}). Fig. 5C showed the plots of anodic peak potential (E_{pc}) and cathodic peak potential (E_{pa}) *versus* the natural logarithm of the scan rate ($\ln v$). Based on the plots, the $\alpha_s n$ was calculated to be 0.496. According to the literature,[38] $0.3 < \alpha < 0.7$, thus the α_s was estimated to be 0.496, and n was estimated to be 1, which demonstrated a single electron transfer. Thus, the possible mechanism involving the direct electrochemical process can be expressed as follows:

$$Cu(OH)_2 + OH^- \rightarrow CuOOH + H_2O + e \quad (3)$$

$$Co(OH)_2 + OH^- \rightarrow CoOOH + H_2O + e \quad (4)$$

$$Ni(OH)_2 + OH^- \rightarrow NiOOH + H_2O + e \quad (5)$$

The above three electrochemical processes happened simultaneously to form the electrochemical behavior, as shown in Fig. 5A. The electron transfer rate k_s could be estimated with Laviron's equation:[38]

$$k_s = \alpha nFv/RT \quad (6)$$

When the scan rate was 0.1 V s^{-1}, the mean value of k_s was calculated to be 1.44 s^{-1}. For comparison, the k_s of Cu–Co–Ni NSs/GCE without CNFs was calculated to be 1.15 s^{-1}, which was smaller than that of Cu–Co–Ni NSs/CNFs/GCE, indicating that the existence of CNFs promote the electron transfer. The electrochemical impedance spectroscopy (EIS) of Cu–Co–Ni NSs/CNFs/GCE (curve a) and Cu–Co–Ni NSs/GCE (curve b) in the presence of 5 mM $Fe(CN)_6^{3-/4-}$ with 0.1 M KCl as the supporting electrolyte have been investigated as shown in Fig. S2 (ESI†). To give more detailed information about the electrical properties of these electrodes, the Randles circuit (inset) was chosen to fit the impedance data. In the Randles circuit, the resistance to charge transfer (R_{ct}) and the diffusion impedance (W) were both assumed in parallel to the interfacial capacity (C_{dl}). This parallel structure of R_{ct} and C_{dl} gave rise to a semicircle in the complex plane plot of Z_{im} against Z_{re}. As shown in Fig. S2 (ESI†), the charge-transfer resistance (R_{ct}) of Cu–Co–Ni NSs/GCE is about 95 Ω. However, the R_{ct} of Cu–Co–Ni NSs/CNFs/GCE (45 Ω) is smaller than that of Cu–Co–Ni NSs/CNFs/GCE. The smaller R_{ct} might result from the good conductivity of CNFs, which improved electron transfer. The result is consistent with CVs, which showed small peak potential separations at Cu–Co–Ni NSs/CNFs/GCE and proved the direct electron transfer of Cu–Co–Ni NSs/CNFs/GCE is superior to that of Cu–Co–Ni NSs/GCE.

3.4. Electrocatalytic properties of the Cu–Co–Ni NSs/CNFs/GCE

The electrocatalytic properties of Cu–Co–Ni NSs/CNFs/GCE were explored as shown in Fig. 6. Fig. 6A shows CVs of the CNFs/GCE (curve a and b), Cu–Co–Ni NSs/GCE (curve c and d) and Cu–Co–Ni NSs/CNFs/GCE (curve e and f) in 0.1 M N_2-saturated NaOH at a scan rate of 0.1 V s^{-1} in the presence (curve b, d and f) and absence (curve a, c and e) of 0.8 mM glucose. It was observed that the anodic peak current of Cu–Co–Ni NSs/CNFs/GCE increased obviously and the cathodic peak was maintained after 0.8 mM glucose was added (curve f), indicating a typical electrocatalytic oxidation process of glucose by high valence state of CuOOH, CoOOH and NiOOH. As a comparison, the CVs of the Cu–Co–Ni NSs/GCE (curve c and d) and CNFs/GCE (curve a and b) in the absence and presence of 0.8 mM glucose were also shown in Fig. 6A. The response of the Cu–Co–Ni NSs/GCE toward the oxidation of glucose was weaker than that of Cu–Co–Ni NSs/CNFs/GCE. And there is no obvious response at the CNFs/GCE to the oxidation of glucose. The results suggested the good catalytic performance resulted from the Cu–Co–Ni NSs on the modified electrode. The reason why the Cu–Co–Ni NSs/CNFs/GCE provided more obvious catalytic activity to glucose than Cu–Co–Ni NSs/GCE is that the CNFs offer an excellent substrate for forming a large number of hierarchical Cu–Co–Ni NSs with a large specific surface area, as shown in Fig. 3. The Cu–Co–Ni NSs/GCE showed a thick film of Cu–Co–Ni NSs, which might result in the poor electrochemical properties. Therefore, the Cu–Co–Ni NSs played an extremely crucial role and the CNFs played a quite important role in the catalytic performance.

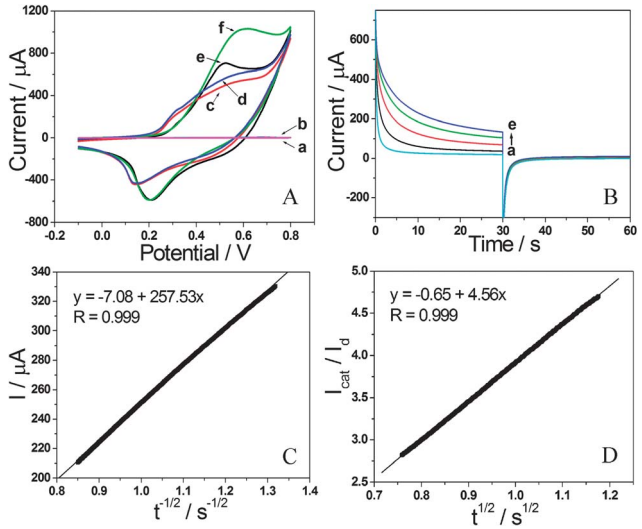

Fig. 6 (A) CVs of CNFs/GCE (a and b), Cu–Co–Ni NSs/GCE (c and d) and Cu–Co–Ni NSs/CNFs/GCE (e and f) in 0.1 M N_2-saturated NaOH at a scan rate of 0.1 V s^{-1} in the presence (b, d and f) and absence (a, c and e) of 0.8 mM glucose. (B) Double steps chronoamperograms of Cu–Co–Ni NSs/CNFs/GCE in 0.1 M NaOH solution with different concentrations of glucose: (a) 0 mM, (b) 1 mM, (c) 2 mM, (d) 3 mM and (e) 4 mM. Potential steps were 500 mV and 300 mV, respectively. (C) Dependency of transient current on $t^{-1/2}$. (D) Dependency of I_{cat}/I_d on $t^{1/2}$ derived from the data of chronoamperograms of curve (a) and (d) in panel (A).

The catalytic rate constant (k_{cat}) of the Cu–Co–Ni NSs/CNFs/GCE was measured with double step chronoamperograms under a suitable working electrode potential. Fig. 6B showed the double step chronoamperograms of Cu–Co–Ni NSs/CNFs/GCE in the absence (curve a) and presence (curve b–e: 1.0–4.0 mM) of glucose. The applied potential steps were 500 mV and 300 mV, respectively. Fig. 6C showed the plot of net current *versus* the minus square roots of time, and presented a linear dependency. It demonstrated that the electrocatalytic oxidation of glucose was a diffusion-controlled process. The diffusion coefficient (D) of glucose could be estimated according to the Cottrell equation:[39]

$$I = nFAD^{0.5}C\pi^{-0.5}t^{-0.5} \quad (7)$$

where C is the bulk concentration. The mean value of the diffusion coefficient of glucose was evaluated to be 5.72×10^{-4} cm^2 s^{-1} using the slope in Fig. 6C.

Chronoamperometry can also be used for the evaluation of the catalytic rate constant with the following equation $\lambda = K_{cat}Ct$:[40]

$$\frac{I_{cat}}{I_d} = \lambda^{0.5}\left[\pi^{0.5}\mathrm{erf}\left(\lambda^{0.5}\right) + \frac{\exp(-\lambda)}{\lambda^{0.5}}\right] \quad (8)$$

where I_{cat} and I_d are the currents in the presence and absence of glucose, respectively, is the argument of the error function, k_{cat} is the catalytic rate constant, and t is elapsed time. In the case where $\lambda > 1.5$, erf($\lambda^{0.5}$) is almost equal to unity, the above equation can be reduced to:

$$\frac{I_{cat}}{I_d} = \lambda^{0.5}\pi^{0.5} = \pi^{0.5}(k_{cat}Ct)^{0.5} \quad (9)$$

From the slope of the plot: I_{cat}/I_d *versus* $t^{0.5}$, as shown in Fig. 6D, the mean value of k_{cat} for glucose was calculated to be 2.2×10^6 cm^3 mol^{-1} s^{-1}. In addition, the chronoamperometric response of Cu–Co–Ni NSs/GCE was also investigated for comparison. The k_{cat} for glucose was calculated to be 8.1×10^5 cm^3 mol^{-1} s^{-1}. The result showed the good conductivity and large specific surface area rendering the CNFs to promote the catalytic effect towards glucose.

Fig. 7A displayed the typical current–time curves of the Cu–Co–Ni NSs/CNFs/GCE (curve a) and the Cu–Co–Ni NSs/GCE (curve b) toward the oxidation of glucose, respectively. The amperometric responses of the sensors were studied by successively adding glucose solutions into the 0.1 M N_2-saturated NaOH under stirring. The oxidation current increased sharply to reach a maximum steady-state value and achieved 95% of the steady-state current (I_{ssc}) within 2 s. The inset of Fig. 7A showed the calibration curves of the sensor, in which the linear range of the glucose detection was from 0.01 to 4.30 mM ($R = 0.996$, $n = 16$) for the Cu–Co–Ni NSs/CNFs/GCE (curve a). The detection limit was estimated to be 3.05 μM based on the criterion of a signal-to-noise ratio (S/N) of 3. For comparison, the amperometric response of the Cu–Co–Ni NSs/GCE (curve b)

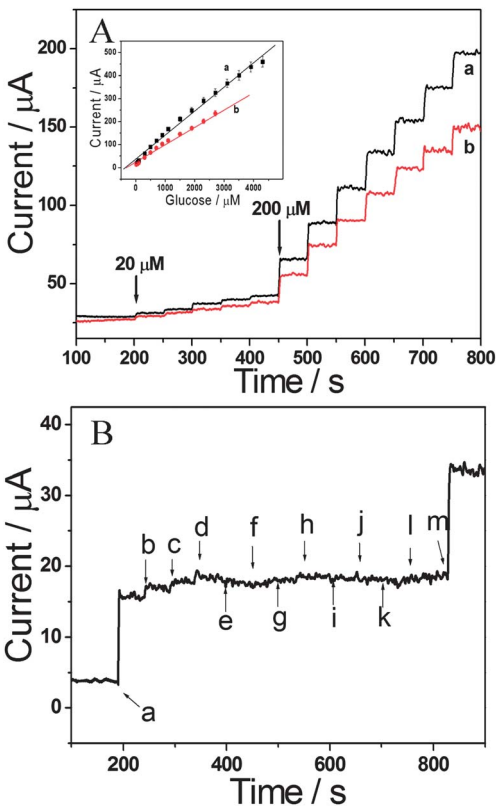

Fig. 7 (A) Typical steady-state current (I_{ssc}) of the Cu–Co–Ni NSs/CNFs/GCE (a) and Cu–Co–Ni NSs/GCE (b) to successive injection of glucose into 10 mL of stirring 0.1 M N_2-saturated NaOH solution at 0.55 V. Inset is the plots of I_{ssc} *versus* glucose concentration. (B) The I_{ssc} of the Cu–Co–Ni NSs/CNFs/GCE to sequential addition of 0.1 mM glucose (a), 0.1 mM UA (b), 0.1 mM AA (c), 0.1 mM sucrose (d), 0.1 mM fructose (e), 0.1 mM lactose (f), 0.1 mM galactose (g), 0.2 mM Na_2SO_4 (h), 0.2 mM KCl (i), 0.2 mM $CaCl_2$ (j), 0.2 mM $FeCl_3$ (k), 0.2 mM NaCl (l) and 0.1 mM glucose (m) into 0.1 M N_2-saturated NaOH solution.

toward the reduction of glucose was also investigated. The linear range of the glucose detection was from 0.02 to 2.70 mM ($R = 0.996$; $n = 12$) with the detection limit of 7.53 μM. The comparison between Cu–Co–Ni NSs/CNFs/GCE and Cu–Co–Ni NSs/GCE confirmed that CNFs could promote the electron transfer and provide a large surface for the growth of the hierarchical Cu–Co–Ni NSs. Therefore, the Cu–Co–Ni NSs/CNFs/GCE exhibited better catalytic activity and sensitivity towards the oxidation of glucose.

Recently, many nonenzymatic glucose sensors based on metal NSs have been reported. A comparison of the performance of our glucose sensor with those reported sensors was listed in Table 1. All of these sensors have their advantages and disadvantages. Generally, the detection limit was fairly low, and the linear range was not wide enough or even very narrow. Taking Cu Pt/Ni–Co NWs electrode[22] as an example, the detection limit was pretty low (0.001 μM), but the linear range was narrow (up to 0.2 mM). Although the detection limit of our sensor is not the lowest, but it is low enough for routine inspection, and the linear range is wider than other sensors.

3.5. Reproducibility, stability and selectivity of the Cu–Co–Ni NSs/CNFs/GCE

The repeatability of the glucose sensor was investigated by successively detecting 200 μM glucose 5 times, a relative standard deviation value (RSD) of 4.19% was calculated for the steady state current. The reproducibility was determined from the response to 200 μM glucose on five different sensors and the RSD was about 2.52%. After the sensor was stored at 4 °C in a refrigerator for 30 days, the current response to 200 μM glucose only decreased by 4.5% of the original current. It is known that interference is inevitable in the determination of some analyses, thus some interferences were also investigated in this work, as shown in Fig. 7B. The interference of organic compounds, including urea acid (UA), ascorbic acid (AA), sucrose, fructose, lactose, galactose, and some common inorganic ions have been investigated. Amperometric response of the sensor to consecutive injection of 0.1 mM glucose, UA, AA, sucrose, fructose, lactose and galactose, 0.2 mM Na_2SO_4, KCl, $CaCl_2$, $FeCl_3$ and NaCl showed that the addition of UA, AA and sucrose provided slight interference for glucose sensing with the RSD of 9.99%, 7.21% and 2.95%, respectively. While 0.1 mM fructose, lactose and galactose, 0.2 mM SO_4^{2-}, K^+, Ca^{2+}, Cl^-, Na^+ and Fe^{3+} showed no obvious interference to glucose detection, which implied that the sensor had good selectivity.

The determination of glucose in blood serum samples was also performed on the Cu–Co–Ni NSs/CNFs/GCE by utilizing the calibration curve method. In brief, the blood samples obtained from hospitalized patients were first diluted with 1 M NaOH (the final solution was adjusted to pH 13), at which time the Cu–Co–Ni NSs/CNFs/GCE was used to monitor the glucose content. The concentration of glucose in blood serum sample was calibrated by standard glucose solution. The standard colorimetric enzymatic procedure was used as a reference for checking the sensor accuracy. The results obtained from the glucose sensor agree well with those obtained by the standard colorimetric enzymatic method. The RSD listed in Table 2 indicates that most of the results are accurate and credible. Thus, it could be concluded that the developed sensor performs very well in the detection of glucose in serum samples.

Table 2 Determination of glucose in blood serum

Samples	Concentration of glucose (mM)			Recovery (%)	RSD (%, $n = 5$)
	Samples found	Added	Found		
1	1.57	0.50	2.16	104.35	4.75
2	1.57	1.00	2.65	103.11	3.40
3	1.57	1.50	3.02	98.37	4.39
4	2.05	0.50	2.67	104.71	3.87
5	2.05	1.00	3.15	103.28	2.94
6	2.05	1.50	3.47	97.75	4.15

Table 1 Comparison of the performance of the non-enzyme glucose electrodes

Electrode	Detection limit (μM)	Linear range (mM)	Slope μA (mmol L^{-1} cm^{-2})	References
Cu–Co–Ni NSs/GCE	7.54	0.02 to 2.70	75.65	This work
Cu–Co–Ni NSs/CNFs/GCE	3.05	0.01 to 4.30	104.68	This work
CuO nanorod[a]	1.2	Up to 1.0	450	41
Co_3O_4 nanofibers[b]	0.96	Up to 2.04	36.25	42
NiO nanofibers[c]	1.28	Up to 1.94	32.91	43
Pt/Ni nanowires[d]	1.5	0.002–2.0	920	44
Cu_2O/SMWNTs[e]	0.2	0.0005–2.5	2143	45

[a] CuO nanorod: CuO nanorod agglomerates were synthesized *via* a simple hydrothermal method in the presence of polyethylene glycol (PEG; M_w 20 000). [b] Co_3O_4 nanofibers: Co_3O_4 nanofibers were fabricated by a two-step procedure consisting of electrospinning and subsequent calcination. The as-prepared electrode (denoted as Co_3O_4 NFs-Nafion/GCE) was immersed in water for 1 h to wet the Nafion layer thoroughly before use. [c] NiO nanofibers: the NiO nanofibers are fabricated by a facile two-step synthetic route consisting of electrospinning and subsequent calcination at 500 °C, then the suspension was dropped onto the surface of GCE. [d] Pt/Ni nanowires: the Pt/Ni nanowires were prepared by pulse electrodeposition of Pt and Ni within a nano-pore polycarbonate (PC) film followed by a chemical etching of the film. Pt and Ni were electrodeposited on the PC template by immersing the GC electrode in a mixture of 1.5 M $NiSO_4$, 5 mM H_2PtCl_6 and 0.4 M H_3BO_3. [e] Cu_2O/SMWNTs: a type of nanospindle-like Cu_2O/straight multi-walled carbon nanotubes (SMWNTs) nanohybrids were synthesized using a simple precipitation procedure. The Cu_2O/SMWNTs suspension was cast onto the surface of the pretreated GC electrode, then the Nafion was dropped onto the surface of the nanohybrids modified electrode and dried at ambient temperature.

4. Conclusions

Trimetallic hierarchical Cu–Co–Ni alloy NSs were electrodeposited on the CNFs/GCE surface. The hierarchical Cu–Co–Ni NSs/CNFS/GCE exhibited good electrochemical and electrocatalytic activity for glucose in 0.1 M NaOH. The detection limit (3.05 μM), linear range (0.01–4.30 mM), sensitivity (104.68 μA mM cm^{-2}) and some kinetic parameters for the oxidation of glucose was obtained using amperometry and chronoamperometry techniques. The sensor showed high selectivity and stability. This approach provided a simple and low cost method to develop a new kind of electrochemical sensor.

Acknowledgements

This work was financially supported by the National Natural Science Foundation of China (21065005, 21165010 and 21101146), the Young Scientist Foundation of Jiangxi Province (20112BCB23006; 20122BCB23013), the Foundation of Jiangxi Educational Committee (GJJ13243 and GJJ13244), the State Key Laboratory of Electroanalytical Chemistry (SKLEAC201310), the State Education Ministry and the Open Project Program of Key Laboratory of Functional Small Organic Molecules (no. KLFS–KF–201214; KLFS–KF–01218).

References

1 J. Wang, *Chem. Rev.*, 2012, **108**, 814–825.
2 A. Mazzuchin, E. J. Thibert, R. J. Walton and E. C. Pedley, *Mikrochim. Acta, Suppl.*, 1971, **2**, 285–289.
3 A. Sixto and M. Knochen, *Talanta*, 2009, **77**, 1534–1538.
4 B. X. Li, Z. J. Zhang and Y. Jin, *Anal. Chim. Acta*, 2001, **1**, 95–100.
5 A. Heller and B. Feldman, *Chem. Rev.*, 2008, **108**, 2482–2505.
6 Y. H. Song, H. Y. Liu, Y. Wang and L. Wang, *Anal. Methods*, 2013, **5**, 4165–4171.
7 Z. Y. Wu, B. Q. Wang, S. J. Dong and E. K. Wang, *Biosens. Bioelectron.*, 2000, **3–4**, 143–147.
8 Y. Liu, M. K. Wang, F. Zhao, Z. A. Xu and S. J. Dong, *Biosens. Bioelectron.*, 2005, **21**, 984–988.
9 N. Q. Dung, D. Patil, T. T. Duong, H. Jung, D. Kim and S. G. Yoon, *Sens. Actuators, B*, 2012, **166**, 103–109.
10 J. J. Xu, J. J. Feng, X. Zhong and H. Y. Chen, *Electroanalysis*, 2008, **20**, 507–512.
11 J. Yang, L. C. Jiang, W. D. Zhang and S. Gunasekaran, *Talanta*, 2010, **82**, 25–33.
12 X. H. Kang, Z. B. Mai, X. Y. Zou, P. X. Cai and J. Y. Mo, *Anal. Biochem.*, 2007, **363**, 143–150.
13 J. Wang and W. D. Zhang, *Electrochim. Acta*, 2011, **56**, 7510–7516.
14 Y. B. Hahn, R. Ahmad and N. Tripathy, *Chem. Commun.*, 2012, **48**, 10369–10385.
15 F. G. Xu, K. Cui, Y. J. Sun, C. L. Guo, Z. L. Liu, Y. Zhang, Y. Shi and Z. Li, *Talanta*, 2010, **82**, 1845–1852.
16 C. Y. Lin, Y. H. Lai, A. Balamurugan, R. Vittal, C. W. Lin and K. C. Ho, *Talanta*, 2010, **82**, 340–347.
17 L. Zhang, H. Li, Y. Ni, J. Li, K. Liao and G. Zhao, *Electrochem. Commun.*, 2009, **11**, 812–815.
18 A. Noorbakhsh and A. Salimi, *Electrochim. Acta*, 2009, **54**, 6312–6321.
19 Y. Y. Song, Z. D. Gao and P. Schmuki, *Electrochem. Commun.*, 2011, **13**, 290–293.
20 E. Jin, X. J. Bian, X. F. Lu and C. Wang, *J. Mater. Sci.*, 2012, **47**, 4326–4331.
21 W. B. Lu, G. H. Chang, Y. L. Luo, F. Liao and X. P. Sun, *J. Mater. Sci.*, 2011, **46**, 5260–5266.
22 L. W. Ji and X. W. Zhang, *Electrochem. Commun.*, 2009, **11**, 795–798.
23 L. Kuai, X. Yu, S. Z. Wang, Y. Sang and B. Y. Geng, *Langmuir*, 2012, **28**, 7168–7173.
24 D. F. Liang, Z. W. Liu, R. D. Hilty and G. Zangari, *Electrochim. Acta*, 2012, **82**, 82–89.
25 Z. G. Zhu, L. Garcia-Gancedo, A. J. Flewitt, H. Xie, F. Moussy and W. I. Milne, *Sensors*, 2012, **12**, 5996–6022.
26 H. B. Noh, K. S. Lee, P. Chandra, M. S. Won and Y. B. Shim, *Electrochim. Acta*, 2012, **61**, 36–43.
27 X. H. Kang, Z. B. Mai, X. Y. Zou, P. X. Cai and J. Y. Mo, *Anal. Biochem.*, 2007, **363**, 143–150.
28 Q. W. Tang, L. H. Jiang, Q. Jiang, S. L. Wang and G. Q. Sun, *Electrochim. Acta*, 2012, **77**, 104–110.
29 W. D. Zhang, J. Chen, L. C. Jiang, Y. X. Yu and J. Q. Zhang, *Microchim. Acta*, 2010, **168**, 259–265.
30 S. S. Mahshid, S. Mahshid, A. Dolati, M. Ghorbani, L. X. Yang, S. L. Luo and Q. Y. Cai, *J. Alloys Compd.*, 2013, **554**, 169–176.
31 S. J. Guo and S. H. Sun, *J. Am. Chem. Soc.*, 2012, **134**, 2492–2495.
32 H. J. Huang, Y. Fan and X. Wang, *Electrochim. Acta*, 2012, **80**, 118–125.
33 H. Q. Hou and D. H. Reneker, *Adv. Mater.*, 2004, **16**, 69–73.
34 Y. H. Song, Z. F. He, H. Z. Zhu, H. Q. Hou and L. Wang, *Electrochim. Acta*, 2011, **58**, 757–763.
35 L. Zheng, J. Q. Zhang and J. F. Song, *Electrochim. Acta*, 2009, **54**, 4559–4565.
36 S. Liu, J. Tian, L. Wang, X. Qin, Y. Zhang, Y. Luo, A. M. Asiri, A. O. Al-Youbi and X. Sun, *Catal. Sci. Technol.*, 2012, **2**, 813–817.
37 L. Zhang, W. J. Yuan and B. Q. Hou, *J. Electroanal. Chem.*, 2013, **689**, 135–141.
38 E. Laviron, *J. Electroanal. Chem.*, 1979, **101**, 19–28.
39 A. J. Bard and L. R. Faulkner, *Electrochemical Methods: Fundamentals and Applications*, John Wiley and Sons, Inc., New York, 2001, p. 156.
40 A. J. Bard and L. R. Faulkner, *Electrochemical Methods: Fundamentals and Applications*, John Wiley and Sons, Inc., New York, 2001, p. 471.
41 C. Batchelor-McAuley, Y. Du, G. G. Wildgoose and R. G. Compton, *Sens. Actuators, B*, 2009, **135**, 230–235.
42 Y. Ding, Y. Wang, L. Su, M. Bellagamba, H. Zhang and Y. Lei, *Biosens. Bioelectron.*, 2010, **26**, 542–548.
43 Y. Ding, Y. Wang, L. C. Zhang, H. Zhang and Y. Lei, *J. Mater. Chem.*, 2012, **22**, 980–986.
44 S. S. Mahshid, S. Mahshid, A. Dolati, M. Ghorbani, L. X. Yang, S. L. Luo and Q. Y. Cai, *Electrochim. Acta*, 2011, **58**, 551–555.
45 X. M. Zhou, H. G. Nie, Z. Yao, Y. Q. Dong, Z. Yang and S. M. Huang, *Sens. Actuators, B*, 2012, **168**, 1–7.